AIAA Propulsion and Energy Forum
19-22 August 2019, Indianapolis, IN
AIAA Propulsion and Energy 2019 Forum

10.2514/6.2019-3828

A Fully Coupled Body Force-Engine Performance Methodology for Boundary Layer Ingestion

Luis López de Vega *, Guillaume Dufour.† and Nicolás García Rosa ‡
ISAE-SUPAERO, Université de Toulouse, Toulouse 31055, France

In reason of their potential improvements in fuel consumption, disruptive propulsion concepts such as Boundary Layer Ingestion are lately earning the attention of the aerospace community. Because of the increased level of multi-disciplinary interactions brought by the tight airframe-propulsor integration, an accurate assessment of this benefit requires a detailed study of the engine behavior from both an aerodynamics and an overall performance standpoint. In this context, this paper presents a fully coupled methodology that integrates a 0D thermodynamic cycle analysis of the core and a 3D body force representation of the fan stage into a single numerical computation. This approach allows to simulate fan-distortion interactions and engine overall performance efficiently in terms of accuracy vs. computational cost trade-off, making it well-suited for conducting full aircraft-engine CFD calculations. The coupling is demonstrated in the assessment of boundary layer ingestion impacts on the small DGEN 380 turbofan. Results provide a quantification of such impacts on fan efficiency, engine power demand, thrust specific fuel consumption, flow distortion transfer and fan aeromechanical response for different levels of engine net thrust.

Nomenclature

a	=	speed of sound
A	=	surface
b	=	metal blockage
C_p	=	specific heat capacity
ΔT_{ISA}	=	ISA temperature offset
e	=	specific internal energy
F_n	=	net thrust
F_{IP}	=	in-plane force
$\measuredangle F_{IP}$	=	in-plane force phase
$\vec{f}$	=	force source term
f_p	=	parallel force source term
f_θ	=	circumferential force source term
γ	=	specific heat ratio
h	=	altitude
h_t	=	specific total enthalpy
K_p	=	non-dimensional parallel force coefficient
K_q	=	non-dimensional heat addition coefficient
$\mathcal{L}$	=	core source term model zone characteristic length
LHV	=	fuel lower heating value
M	=	Mach number
N	=	spool speed
η	=	isentropic efficiency
Ω	=	core source term model zone volume
P	=	engine power

*PhD researcher, Department of Aerodynamics, Energetics and Propulsion; 10 Avenue Édouard Belin, 31055 Toulouse, France; luis.lopez-de-vega@isae-supaero.fr
†Associate Professor, Department of Aerodynamics, Energetics and Propulsion
‡Associate Professor, Department of Aerodynamics, Energetics and Propulsion

p = static pressure
p_t = total pressure
π = total pressure ratio
Q = heat source term
R = gas constant
r = radius
ρ = density
τ = spool torque
T = static temperature
T_t = total temperature
$\vec{V}$ = velocity vector
V = velocity magnitude
W = massflow
W_F = fuel flow
y^+ = non-dimensional wall distance

Subscripts

L = low speed
∞ = flight conditions
0 = boundary layer upstream conditions
2 = fan inlet face
13 = bypass duct
18 = bypass nozzle outlet
21 = core inlet
7 = core nozzle inlet
8 = core nozzle outlet
nom = nominal
ovr = overall
$prop$ = propulsive
th = thermal

Superscripts

$*$ = target value

I. Introduction

The economic and environmental constraints imposed to the civil aviation market have made fuel burn reduction a major concern in the design of new aircraft. In this context, emerging propulsion concepts such as Boundary Layer Ingestion (BLI) are being considered as a means to achieve this target. In a BLI configuration the engines are embedded into the airframe, ingesting boundary layer low-momentum fluid and homogenizing the aircraft wake. These effects decrease the flight power requirement and the thrust specific fuel consumption with respect to a podded-engine configuration [1–3]. However, predicting the gains of this disruptive architecture is a complex task as it requires to account for overall engine performance, fan response to inlet distortion, aircraft external aerodynamics and the coupling existing between these disciplines.

Many contributions have considered the assessment of BLI effects. From a system-level perspective, thermodynamic cycle models have been applied to identify key impacts on powerplant and aircraft performance [4–7], but the detailed fan aerodynamic response to inflow distortion was not modeled. From the aerodynamics standpoint, boundary layer ingesting fans have received a lot of attention, with various levels of fidelity. Using full-annulus URANS simulations, Fidalgo et al. [8] and Gunn and Hall [9] provided a description of the flow mechanisms of fan-distortion interaction. Lower-fidelity modeling approaches, such as actuator disk methods [1, 10, 11] and particularly body force models [12–16] have shown a good accuracy in reproducing the main features of distortion transfer and overall impact on fan performance. However, none of the mentioned contributions actually examines the coupling between fan aerodynamics and engine performance.

In the literature, a method that couples aerodynamic and engine performance analysis is the so-called *zooming* approach, mainly aimed at improving the accuracy of individual component representation in overall performance models. This improvement is achieved through CFD calculations of a turbomachinery component, which can range from one-dimensional mean line calculations [17–20], to 3D CFD simulations [21–23], or some intermediate levels such as 2D streamline curvature models [24]. In these contributions, CFD data is used to re-scale component maps in the performance model, hence enhancing the predictions of the latter over a specific engine operation range. Based on the zooming concept, approaches where the component performance map is fully replaced by a concurrently-run CFD simulation have also been proposed. In the particular case of fan component modeling, 3D single-passage mixing-plane computations of the fan stage were used by Pilet et al. [25] to study sub-idle engine operation. Nevertheless, none of these approaches is suited for BLI studies, as their application in the framework of aircraft-engine integration is not straightforward and full-annulus simulations are required to account for distortion transfer.

In this context, the present work aims at proposing a methodology that: (i) fully couples the fan aerodynamics and the engine performance modeling, (ii) is suited for integrated aircraft-engine studies, such as BLI configurations and (iii) is computationally affordable and can be applied in daily design loops. To this end, a PROOSIS-based [26] engine core performance model and a CFD computation of the engine aerodynamics are fully coupled. The simulation of the 3D fan stage aerodynamics is achieved through a body force modeling approach, providing an accuracy comparable to full-annulus URANS simulations, but at a fraction of their computational cost [13, 14, 27]. To make the approach suited for integrated studies, a simple source term model is proposed to represent the core, thus allowing the flows exhausting from both the core and bypass nozzles to be naturally accounted for in the CFD calculation. From the user standpoint, the overall simulation is driven by specifying one engine performance parameter such as thrust or fuel massflow. This approach is implemented in the FlowSimulator environment [28] and completely automates all the information exchanges between the aerodynamic and performance models. The methodology is demonstrated in the assessment of BLI effects on a small turbofan aero-propulsive performance.

The paper is organized as follows. Section II describes the test case, the models, the algorithm, the implementation and the metrics of the coupling methodology. Section III presents a validation of the coupling against a thermodynamic cycle calculation for nominal engine operation. In section IV, the effects of BLI are assessed in terms of overall engine performance, fan stage aerodynamics and fan aeromechanical behavior. Conclusions and perspectives are discussed in section V.

II. Methodology

The present approach relies on coupling a CFD simulation and an engine performance model. The engine inflow, the fan stage and the bypass nozzle are simulated by a full-annulus body force approach. The core flow of the engine is represented by a simple source term model, followed by the exhaust core nozzle. The body force model is derived from the blade row geometry and calibrated using reference CFD results, and the model input (rotational speed) is transferred from the performance model simulation. The source terms of the core model are set to match the thermodynamic variations calculated by the performance model. In the latter, the engine inflow and fan stage are replaced by averaged CFD data. The CFD computation and the engine models are run sequentially and exchange information until convergence is reached. This section first presents the test-case used, the DGEN 380 turbofan. Then, the different models are described, as well as the implementation of the coupling algorithm and the definition of the engine performance metrics considered in this study.

A. DGEN 380 turbofan

The DGEN 380 is a small turbofan developed by Price Induction, now AKIRA Technologies. It features a two-spool, unmixed flow architecture and is intended to motorize 4 to 5-seat personal light jets at a cruise altitude of 10000 ft and Mach number of 0.35. The 14-inch fan stage consists in 14 rotor blades and 40 outlet guide vanes (OGV). The engine core comprises a centrifugal compressor driven by a single-stage high pressure turbine, a reverse-flow combustion chamber and a single-stage low-pressure turbine driving the fan through a gearbox. The station nomenclature is depicted in figure 1. A fully instrumented version of this engine is available at the ISAE-SUPAERO turbofan test facility.

B. Performance model

Engine performance is modeled through a 0D thermodynamic cycle calculation of the core section using the gas turbine simulation tool PROOSIS. Turbomachinery components are represented through compressor and turbine maps

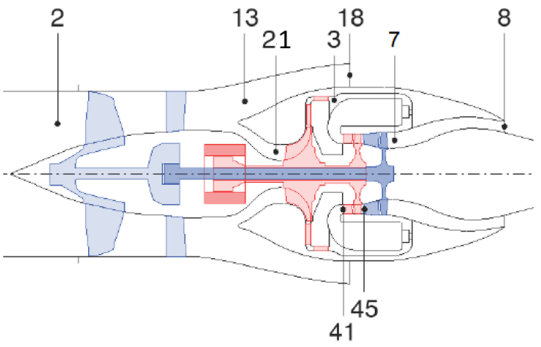

Fig. 1 Station nomenclature of the DGEN 380 turbofan (adapted from [25])

derived either from previous CFD simulations or through a scaling procedure. BETA-type and ZETA-type [26] maps are used for the fan and high pressure compressor and the turbines, respectively. As depicted in figure 2, the core model of the DGEN turbofan is derived from the whole engine model and gathers all components from stations 21 to 8, namely the high pressure compressor, the combustion chamber, the high and low pressure turbines, the primary nozzle, the high and low pressure spools and the gearbox. Furthermore, nozzle aerodynamic coefficients are derived from CFD computations and included in the performance model.

To drive the simulation, the user only specifies the fuel flow rate (W_F), thus setting the core throttle. The outlet static pressure (p_8) is derived from the flight conditions and the nozzle total-to-static pressure ratio. In terms of information exchange in the coupled approach: (i) the total conditions at station 21 (p_{t21}, T_{t21}) and the torque applied to the low pressure spool (τ_L) are retrieved from the fan stage flow simulation and (ii) the fan rotational speed (N_L) and the total conditions at station 7 (p_{t7}, T_{t7}) from the engine model are transferred to the global CFD simulation to update the aerodynamic source term models.

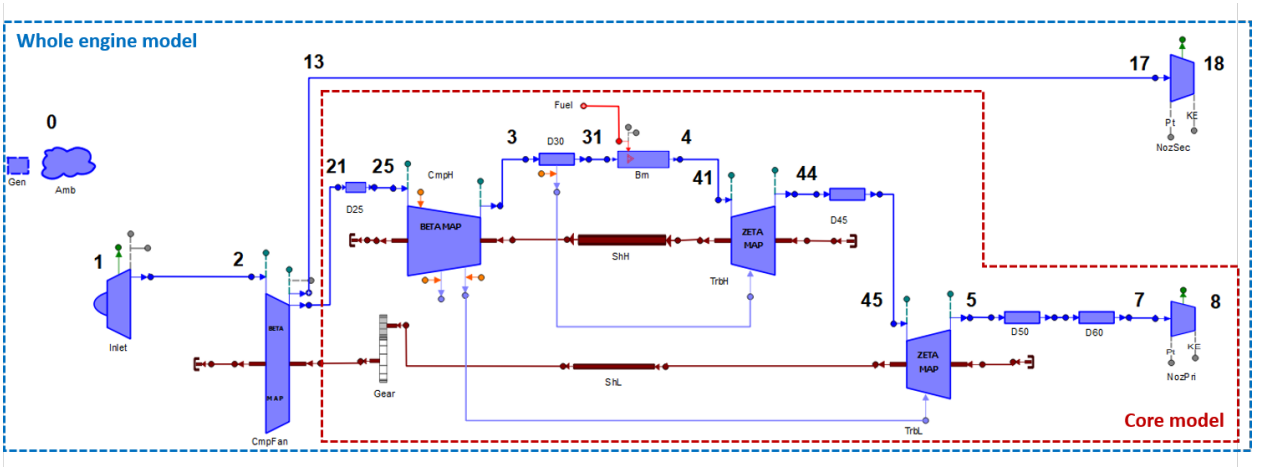

Fig. 2 Performance model of the DGEN 380 turbofan

C. Aerodynamic model

Engine internal aerodynamics are accounted for using a source term modeling approach rather than actually meshing the rotating parts. In turbomachinery applications this technique is known as *body force modeling* and greatly reduces the computational cost of simulations due to a reduced number of mesh cells and the possibility to handle distorted inflow cases with a steady approach, while providing an accuracy comparable to full-annulus URANS simulations [14, 15, 29]. Body force modeling is applied in the fan stage whereas a simple source term model is used in the core section.

A meridional view of the aerodynamic model is depicted in figure 3. It includes the inlet duct, spinner, rotor and

OGV swept volumes and the core and bypass nozzle outlet sections, which are sized according to their actual values. As no detailed representation of the core aerodynamics is sought, the contours defined between station 21 and 7 and the position of the core model zone are arbitrary.

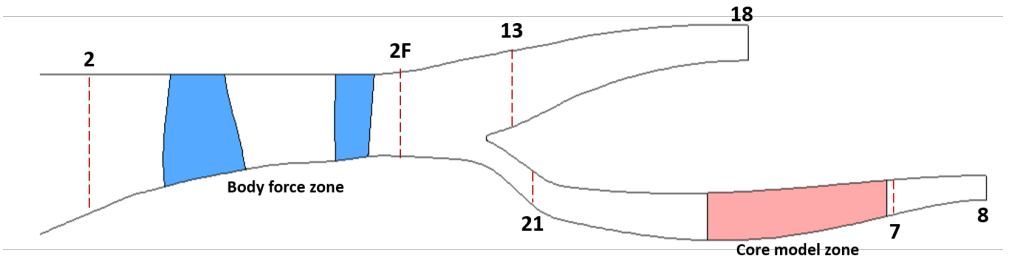

Fig. 3 Aerodynamic model of the DGEN 380 turbofan

1. Fan stage body force modeling

The key idea of body force modeling is to replace the rotor and OGV rows by a volume source field that is active in the region swept by the blades and reacts to local flow conditions, providing the same flow turning and entropy rise as the actual blades. In this contribution, the Lift/Drag model of Thollet [14] is applied to the fan stage. The model calibration coefficients are obtained from a single passage, mixing-plane computation at the nominal operating point. Body force predictions of isolated fan performance over the nominal speedline are compared to mixing-plane computation results in figure 4, showing the capability of the model to reproduce conventional calculations.

Once the body force model is calibrated, the computation of the volume source field only requires to specify the fan rotational speed (N_L) which is retrieved from the core thermodynamic cycle calculation.

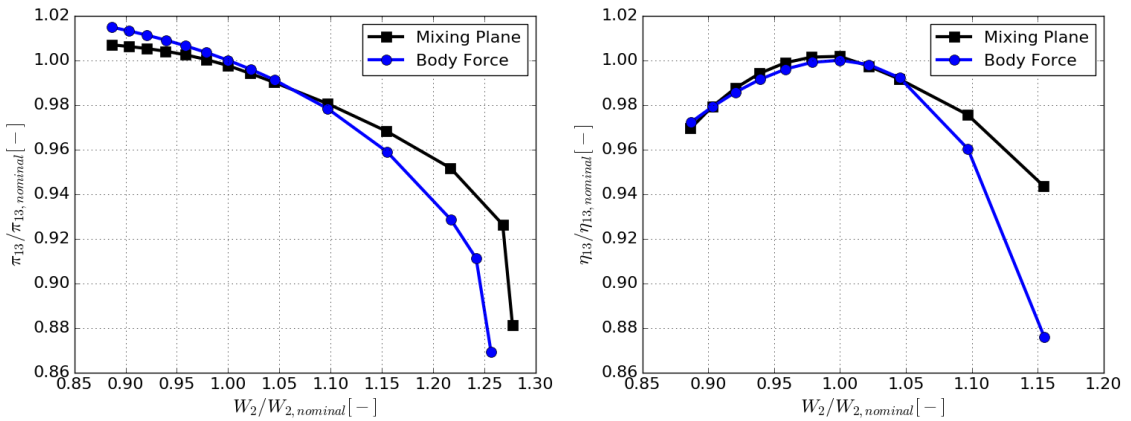

Fig. 4 Fan performance prediction using the body force modeling approach

2. Core section source term modeling

Engine core aerodynamic effects are modeled as a total pressure and total temperature rise between stations 21 and 7, and a massflow addition to account for fuel injection in the combustion chamber. For this purpose, a source term model inspired by the body force technique is proposed. This model locally computes the source terms required to reach homogeneous values of total pressure and total temperature at the core nozzle inlet (station 7). Then, the mass flow in the core section is naturally established resulting from the total conditions at station 7 and the mass flow addition provided by the source term model. The model inputs (p^*_{t7}, T^*_{t7} and W_F) are provided by the 0D thermodynamic cycle calculation.

3. Governing equations

The body force and core source term models are included in the RANS equations by means of right hand-side terms (viscous and heat transfer terms are omitted for clarity):

$$\frac{\partial \mathbf{M}}{\partial t} + \nabla \cdot (\mathbf{M}\vec{V}) = \nabla \cdot \mathbf{N} + \mathbf{F} \tag{1}$$

where:

$$\mathbf{M} = \begin{bmatrix} \rho \\ \rho\vec{V} \\ \rho(e + V^2) \end{bmatrix}, \mathbf{N} = \begin{bmatrix} \vec{0} \\ -pI \\ -p\vec{V} \end{bmatrix} \tag{2}$$

and $\mathbf{F}$ stands for the body force source terms $\mathbf{F}_{BF}$ in the body force zone or the core source terms $\mathbf{F}_{CST}$ in the core model zone. The source terms read:

$$\mathbf{F}_{BF} = \begin{bmatrix} -\frac{1}{b}(\rho\vec{V} \cdot \nabla b) \\ -\frac{1}{b}(\rho\vec{V} \cdot \nabla b)\vec{V} + \rho\vec{f} \\ -\frac{1}{b}(\rho\vec{V} \cdot \nabla b)h_t + \rho f_\theta Nr \end{bmatrix}, \mathbf{F}_{CST} = \begin{bmatrix} \frac{W_F}{\Omega} \\ \frac{W_F}{\Omega} \cdot \vec{V} + \rho f_p \cdot \vec{V}/V \\ \frac{W_F}{\Omega} \cdot h_t + \rho f_p \cdot V + Q \end{bmatrix} \tag{3}$$

In the body force model, b is the metal blockage and $\vec{f}$ is the force field representing the blade effects. A detailed description of both terms is out of the scope of this contribution and can be found in [14].

Regarding the core source term model, the term W_F/Ω accounts for the fuel mass flow addition with Ω being the volume in which the core source terms are applied. The scalar f_p acting in the momentum and energy equations is a force parallel to the local velocity vector that introduces a total pressure and total temperature rise. Finally, the heat addition term Q in the energy equation accounts for a complementary total temperature increase. The relations for the parallel force and heat addition on the local flow variables are derived on Hooke's law and dimensional analysis and read:

$$f_p = \frac{K_p}{\rho\mathcal{L}}(p^*_{t7} - p_t) \tag{4}$$

$$Q = \rho C_p \frac{K_q}{\mathcal{L}}(T^*_{t7} - T_t)V \tag{5}$$

where the values of p^*_{t7} and T^*_{t7} are the target values of total conditions at station 7 obtained from the 0D thermodynamic cycle simulation and constitute the source term model inputs. The non-dimensional coefficients K_p and K_q are constants that control the intensity of the response of the model to the local flow conditions and $\mathcal{L}$ is the characteristic length of the core duct.

4. Numerical settings

All CFD simulations in the present contribution are carried out using an implicit pseudo-time marching scheme to reach the steady state solution, along with a V-cycle multigrid technique for convergence acceleration. Convective fluxes are treated using a second-order Roe scheme with the Van-Albada limiter. Turbulence closure is achieved using the Spalart-Allmaras model.

D. Coupling implementation

The coupling between the CFD simulation and the core performance model is implemented in the FlowSimulator [28] environment. The elsA [30] CFD solver and external python-based modules for the body force and core source term models are coupled in-memory with a pre-compiled executable containing the PROOSIS-based performance model. A python wrapper handles the information exchange between the CFD solver, the executable containing the core model and the external python modules containing the body force and core source term models. In addition, integrated tools based on the Antares libary [31] are used to compute averaged values of the flow variables required by the performance model. In particular, stagnation quantities are mass-averaged [32] and used to compute derived variables such as fan

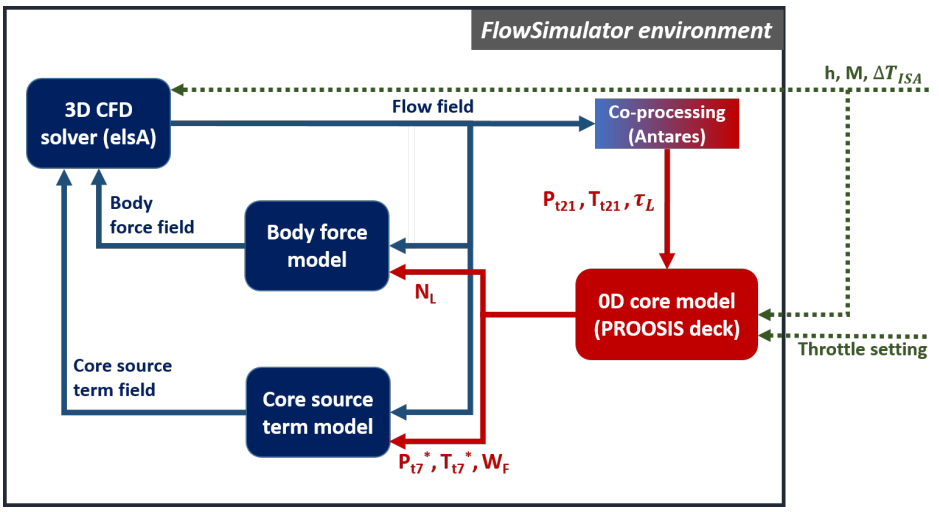

Fig. 5 Coupling implementation in the FlowSimulator environment

power and spool torque. This coupling process is depicted in figure 5 and is driven externally by setting the flight conditions (h, M, ΔT_{ISA}) and the engine throttle setting through the fuel flow rate (W_F).

During a coupled simulation, the 3D flow field obtained from the CFD computation is periodically co-processed to obtain the 0D values of core inlet total conditions and low pressure spool torque required by the performance model to calculate the core operating point. Resulting values of low pressure spool speed and total conditions in the primary nozzle plus fuel flow rate are used to update both the body force and the core source term models. Typically, around 10 updates are sufficient for the CFD simulation to provide a converged solution in which the fan power calculated by the body force model is balanced by the low pressure spool power predicted by the thermodynamic cycle simulation. An advantage of this process chain lies in the fact that the updates only affect the aerodynamic model inputs, while the CFD boundary conditions remain unchanged during the whole simulation. This last point constitutes a major difference with respect to previous zooming approaches [21–23, 25].

E. Engine performance metric definition

Engine performance parameters are computed using averaged values of the CFD simulation. Additionally, the computation of the net thrust and engine power requires to account for the engine inlet velocity, whose definition is ambiguous here as the engine external aerodynamic flow is not simulated. In this contribution an equivalent engine inlet velocity V_0 is derived from station 2 conditions assuming that the stream tube entering the engine follows an isentropic transformation from ambient conditions to this station (i.e., $p_{t0} = p_{t2}$, $T_{t0} = T_{t2}$ and $p_0 = p_\infty$):

$$V_0 = a_0 \cdot M_0 \tag{6}$$

with:

$$M_0 = \sqrt{\frac{2}{\gamma - 1}\left[\left(\frac{p_{t0}}{p_0}\right)^{\frac{\gamma-1}{\gamma}} - 1\right]}, \quad T_0 = \frac{T_{t0}}{1 + \frac{\gamma-1}{2}{M_0}^2}, \quad a_0 = \sqrt{\gamma R T_0} \tag{7}$$

Engine net thrust, power and thrust specific fuel consumption (TSFC) are then defined as in equations 8, 9 and 10 respectively:

$$F_n = [W_{18}V_{18} + A_{18}(p_{18} - p_0)] + [W_8V_8 + A_8(p_8 - p_0)] - W_2V_0 \tag{8}$$

$$P = \left(W_{18}\frac{V_{18}^2}{2} + W_8\frac{V_8^2}{2}\right) - W_2\frac{V_0^2}{2} \tag{9}$$

$$TSFC = \frac{W_F}{F_n} \tag{10}$$

Propulsive efficiency (η_{prop}), thermal efficiency (η_{th}) and overall efficiency (η_{ovr}) are derived from the previous definitions:

$$\eta_{prop} = \frac{F_n \cdot V_\infty}{P}\,, \quad \eta_{th} = \frac{P}{W_F \cdot LHV}\,, \quad \eta_{ovr} = \frac{F_n \cdot V_\infty}{W_F \cdot LHV} = \eta_{prop} \cdot \eta_{th} \tag{11}$$

III. Validation for nominal engine operation

The coupled body force-engine performance approach is first validated in the prediction of engine performance under clean inflow conditions. In this regard, a 0D thermodynamic cycle calculation of the whole engine performance model (including the fan component, as depicted in figure 2) is compared to a coupled simulation using a single passage version of the computational domain presented in figure 3. The associated structured, multi-block mesh features 420k cells with $y^+ < 1$ at the solid wall boundaries. Both simulations are compared in the operating point used for scaling the performance model maps, summarized in table 1. Carrying out the validation in this operating point allows to remove inaccuracies in the thermodynamic cycle calculation due to interpolations in the turbomachinery characteristic maps. Therefore, disagreements between both simulations can be attributed exclusively to the coupling algorithm or to the flow averaging procedures.

The comparison between the coupled and the thermodynamic cycle computations is displayed in figure 6, taking the results of the latter as a reference. For some of the most relevant engine performance parameters and efficiencies, differences remain below 0.15% and 0.6%, respectively. These discrepancies are considered to be acceptable and indicate a correct integration of the different levels of fidelity and dimensionality of the performance and aerodynamic models into a single, multi-disciplinary simulation.

$\mathbf{h}[ft]$	$\mathbf{M}[-]$	$\Delta\mathbf{T}_{ISA}[K]$	$\frac{\mathbf{W}_F}{\mathbf{W}_{F,nom}}[-]$
10000	0.35	0.0	1.0

Table 1 Map scaling operating point definition

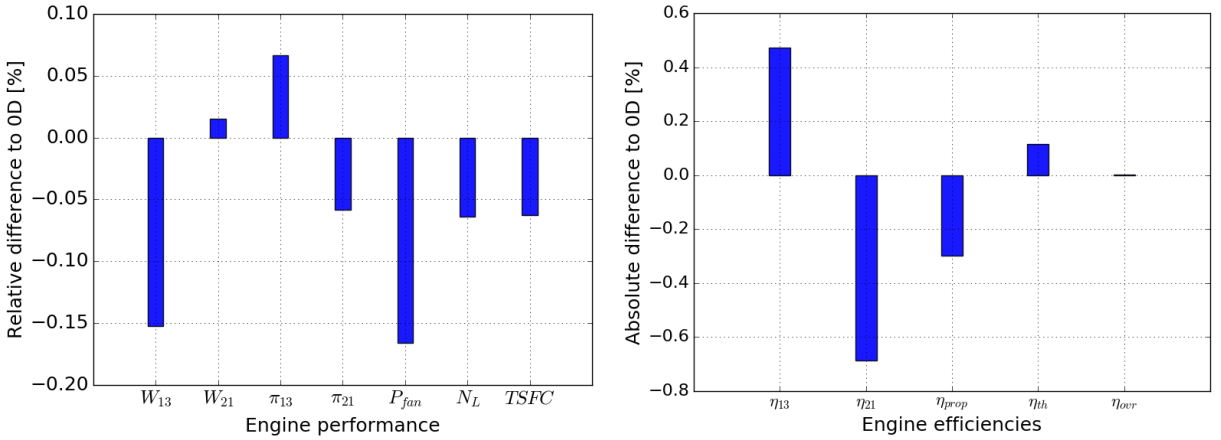

Fig. 6 Comparison of results from the performance model and the coupled simulations

IV. Assessment of BLI effects

In this section the coupled methodology is applied to a BLI configuration in order to assess the impact of fan-inflow distortion interaction on engine overall performance (subsection IV.A), internal aerodynamics (subsection IV.B) and

aeromechanical response (subsection IV.C). To this end, a vertically stratified total pressure distribution with a spatial extent of 30% of the inlet diameter is imposed at the inlet of a full-annulus computational domain, about one fan diameter upstream of station 2. As both nozzles remain unchoked for the study presented here, static pressure outflow boundary conditions are set at the domain outlet (sections 8 and 18). The associated structured, multi-block mesh features around 25M cells with $y^+ < 1$ at the solid wall boundaries. The effects of this distortion are explored for the altitude and Mach number displayed in table 1 and five levels of engine net thrust, ranging from 80% to 130% of its nominal value. Figure 7 depicts a meridional view of the computational domain and illustrates how the fan body force and core source term models reproduce local aerodynamic effects of boundary layer ingestion. Approximately 6 hours of computational time using 120 CPUs on a HPC cluster were necessary to reach convergence, per thrust level.

In this study, the distortion pattern is assumed to remain unchanged along the engine operating range as the airframe-engine aerodynamic interactions are not modeled. Under this hypothesis, the averaged total pressure drop at the engine inlet is driven by the fan-distortion interaction, resulting in larger decreases with higher thrust levels as depicted in figure 8. However, the observed trend should not be generalized as the coupling effects with external aerodynamics are not considered. Note that the application of the present methodology to aircraft-engine configurations is straightforward, as this would only require to adapt the computational domain to include the airframe.

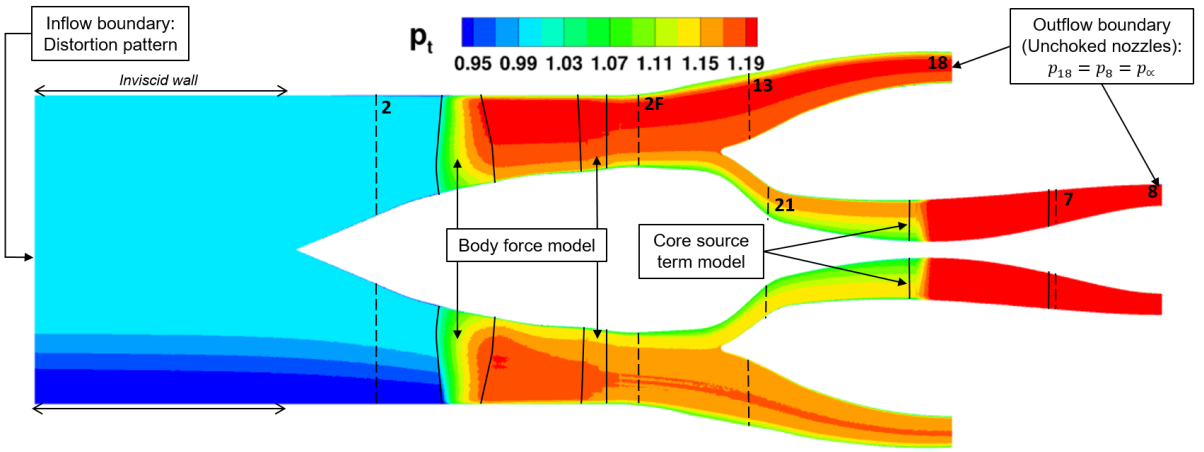

Fig. 7 Meridional view of the coupled simulation results for $F_n/F_{n,nom} = 1.3$. Contours of total pressure normalized by free stream total pressure

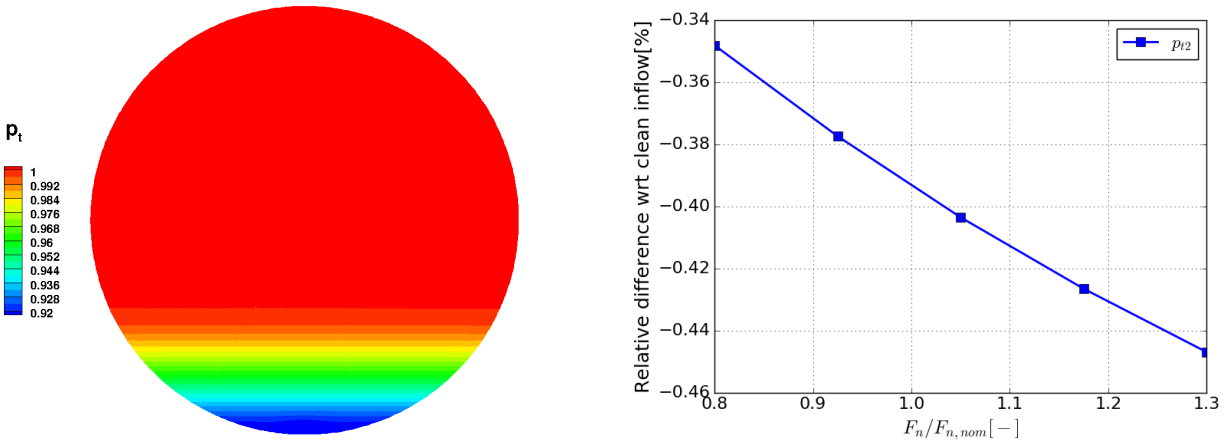

Fig. 8 Inlet distortion profile and induced averaged total pressure drop

A. BLI impact on overall engine performance

Figure 9 shows the impacts of inflow distortion on fan performance. As depicted in the left-hand side plot, inflow distortion translates into an inlet momentum decrease of roughly 1.2%, with twofold effects. On the one hand, lower inlet momentum is responsible for the beneficial reduction of engine power demand to reach a given net thrust in a BLI configuration [1, 12]. On the other hand, the fan surge margin is reduced due to the combination of this massflow reduction and the distortion impact on fan stability limit. The fan spool speed is slightly reduced, and the drop in the bypass ratio indicates that the inlet momentum deficit mainly affects the bypass section. In addition to this, inflow distortion causes a reduction of the fan isentropic efficiency along the whole span which can be measured in the bypass duct (station 13) and core inlet (station 21). This loss is more pronounced in the bypass duct, where the efficiency drops about 0.8% for all the thrust settings considered. In the core section, the efficiency drop is lessened with higher thrust levels. Figure 10 provides an assessment of BLI benefits in terms of engine efficiencies, power requirement and TSFC. As a consequence of the fan efficiency drop, thermal efficiency decreases about 0.1%. On the contrary, the propulsive efficiency is improved by almost 0.6% due to the inlet momentum deficit, as can be seen in the decrease of engine power demand to reach a given thrust. Altogether, these effects lead to an enhancement of the overall efficiency that results in up to a 0.8% gain in TSFC.

Overall, it can thus be concluded that the impact of BLI on global engine performance metrics is not significant for a fixed thrust requirement, as the gains remain below 1%. Therefore, for an embedded engine propulsive architecture, the gain will mostly come from a reduction in the thrust requirement [3] as compared to a podded-engine configuration.

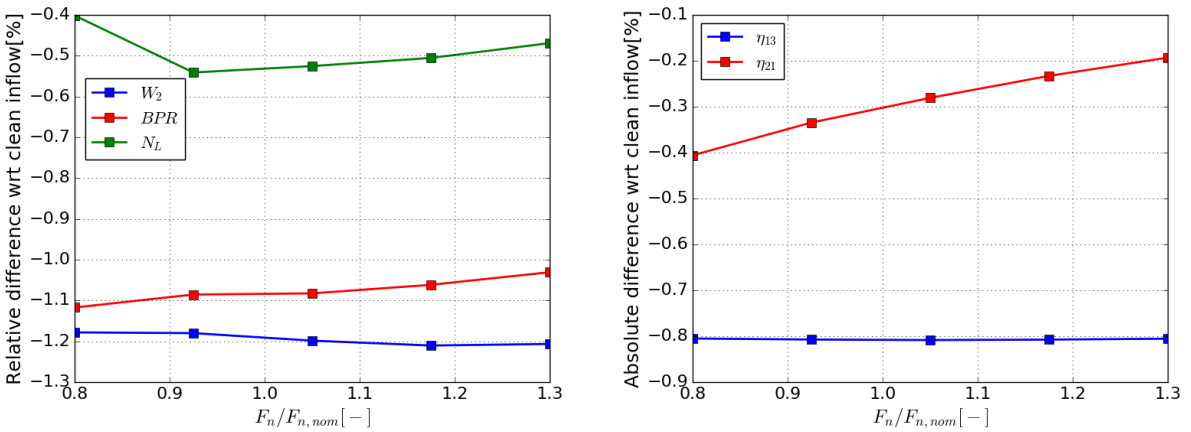

Fig. 9 BLI effect on fan performance

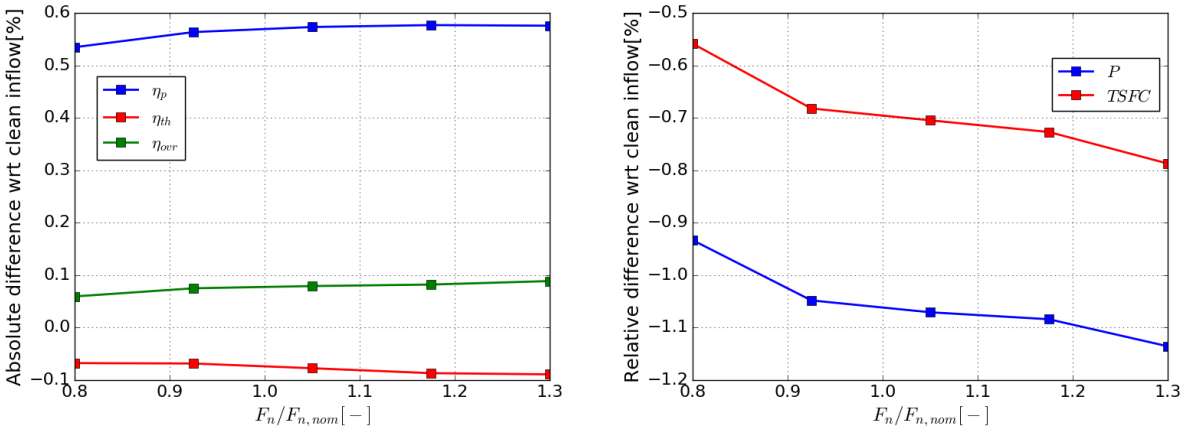

Fig. 10 BLI effect on engine performance

B. BLI impact on fan stage aerodynamics

Contours of total pressure are depicted in figure 11 for station 21 and in figure 12 for station 13. As investigated by Gunn and Hall [9], the non-zero absolute swirl angle induced upstream of the rotor section and the axial velocity deficit result in off-design incidences for both the rotor and OGVs, leading to increased losses and inhomogeneous work input in the annulus. As a result, the inlet distortion pattern is modified and convected through the fan stage.

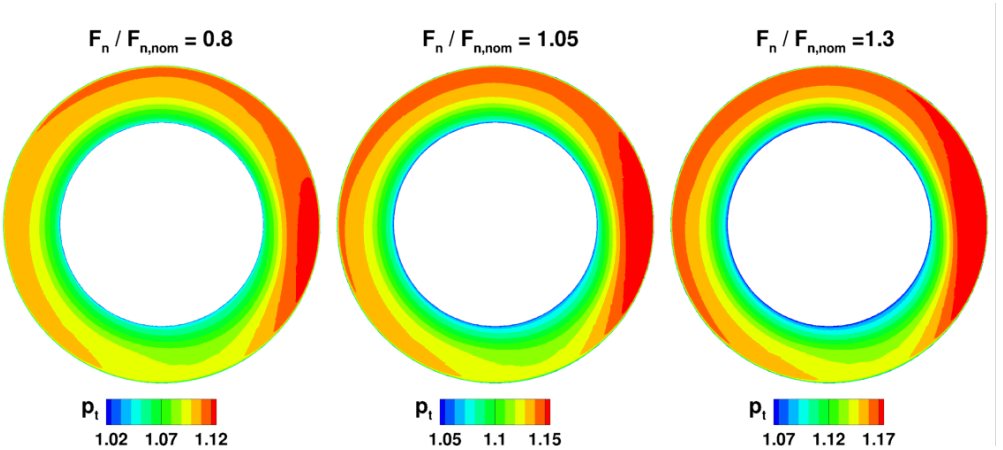

Fig. 11 Contours of total pressure at station 21. Values normalized with free stream total pressur

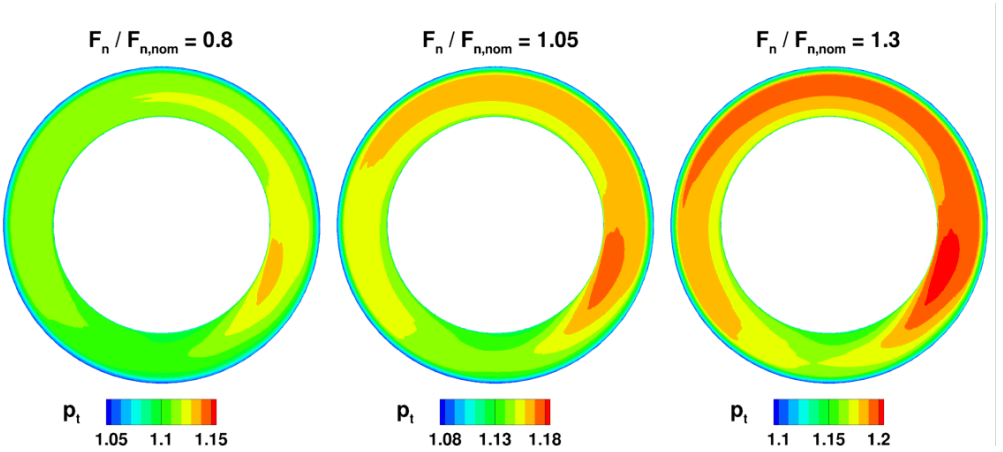

Fig. 12 Contours of total pressure at station 13. Values normalized with free stream total pressure

Of particular interest is the fact that the core inlet (station 21) presents an inhomogeneous flow. This is a consequence of the radial flow redistribution observed by Gunn and Hall [9] and Thollet [14], which tends to increase the distortion near the hub through the rotor. To quantify this redistribution effect, a modal analysis as presented by Thollet [14] is applied. To this end, the frequency content of the total pressure circumferential distributions at relative spans of 20% (near hub) and 80% (near tip) is obtained by computing their Discrete Fourier Transform. Figure 13 displays the spatial mode numbers and the amplitudes of total pressure at the inlet (station 2), OGV exit (station 2F), bypass duct (station 13) and core inlet (station 21) *. At the fan inlet face (station 2), the near-hub flow presents uniform values of total pressure (all modes equal zero), as its span position is lower than the location of the inflow distortion. Flow redistribution effects can be appreciated after the fan stage (station 2F), with the near-hub location presenting non-zero amplitude of the modes. On the contrary, the amplitudes of the near-tip modes are reduced at this station, which indicates that the rotor has attenuated the distortion in this region. Distortion is then convected downstream to stations 13 and 21, remaining almost unaltered despite the presence of the bypass-core splitter.

*note that spatial mode 0 is neglected as it represents the average value of this variable at a given span

This observation shows the importance of accounting for 3D fan aerodynamics in the assessment of BLI configurations. Because of the fan-distortion interaction, the core inlet section of a conventional turbofan might be distorted even for a small proportion of ingested low-momentum fluid. Larger distortions might have a significant negative impact on core performance and operability, potentially outweighing aerodynamic benefits. Accurately capturing the 3D flow field features becomes thus essential to predict such phenomena.

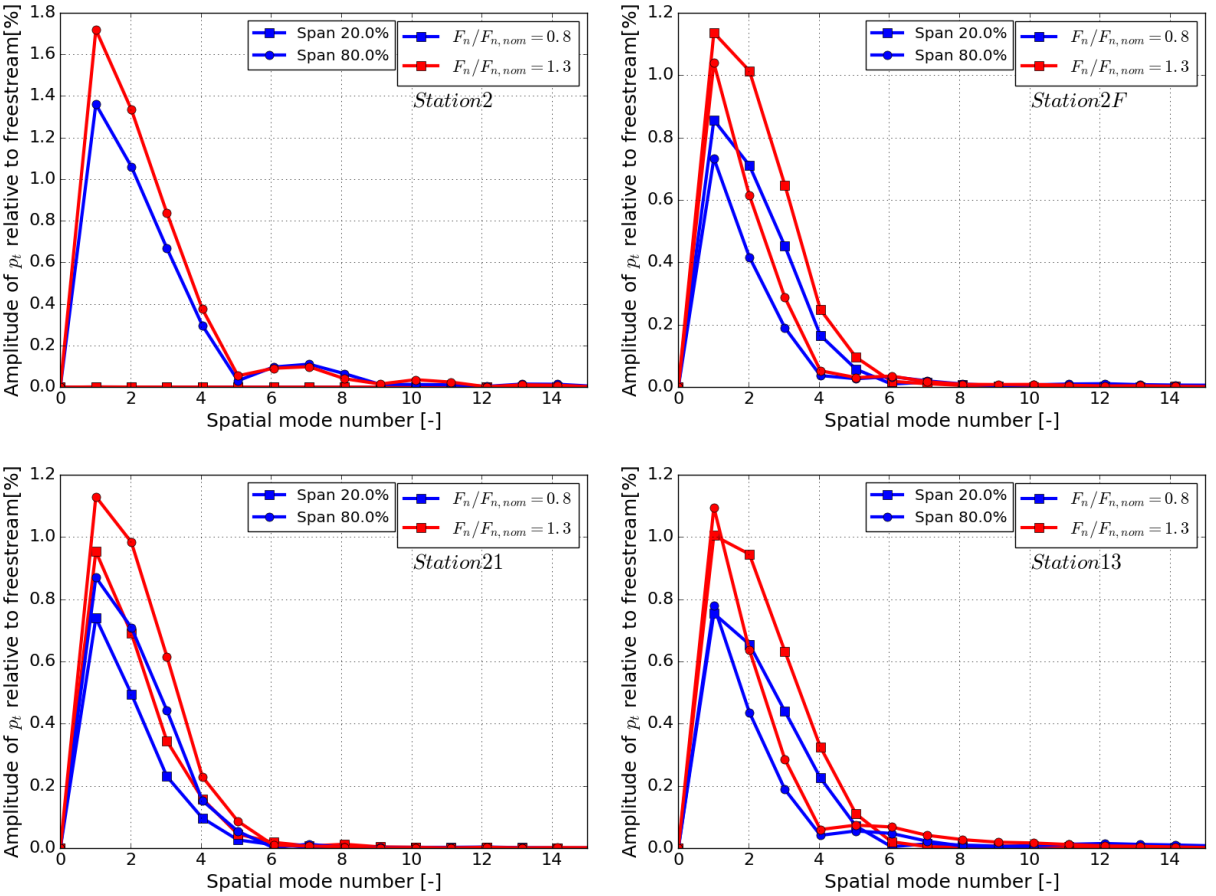

Fig. 13 Modal analysis of total pressure azimuthal profiles at stations 2, 2F, 21 and 13 for thrust levels of $F_n/F_{n,nom} = 0.8$ and $F_n/F_{n,nom} = 1.3$

C. BLI impact on fan aeromechanics

Besides performance and aerodynamic effects, BLI arises new aeromechanical challenges. In particular, the inhomogeneous blade loading around the annulus results in a mechanical solicitation contained in the plane orthogonal to the rotation axis, referred to as in-plane force (F_{IP}) and depicted in figure 14. This force acts on the fan spool and must be accurately predicted to ensure an adequate sizing of the engine mechanical components. In this approach, the integration of the body force field in the rotor and OGV rows allows to retrieve the time-averaged value of the magnitude and phase of the in-plane force.

Figure 15 characterizes the evolution of this solicitation in the fan stage. The force magnitude in the rotor ranges between 2% to 3% of the net thrust provided by the engine, and this figure drops when the throttle setting is increased. Conversely, in the OGV row the force magnitude is roughly a constant fraction of about 1.2% of the net thrust. The analysis of the phase indicates that the in-plane force points upwards in the rotor and downwards in the OGV, with almost unaltered values for the throttle settings considered.

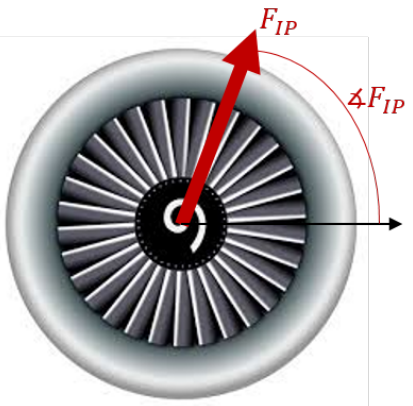

Fig. 14 In-plane force definition

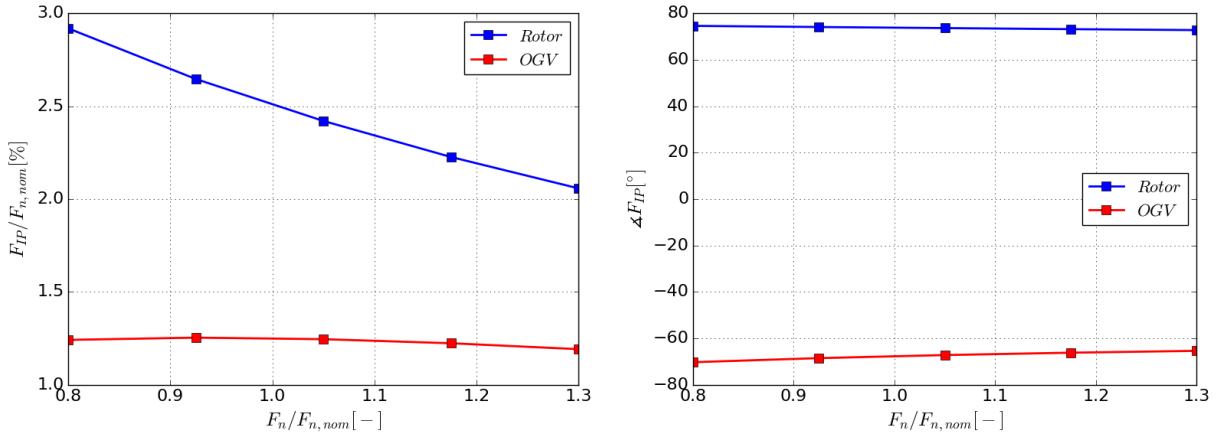

Fig. 15 In-plane force magnitude and phase evolution with thrust level

V. Conclusion

In this contribution, a coupled body force-engine performance approach has been introduced to simultaneously predict fan stage aerodynamics and overall engine performance in Boundary Layer Ingestion (BLI) configurations. The methodology is based on a reduced-order representation of the engine internal aerodynamics using the body force technique, coupled with a thermodynamic cycle model to account for core performance. Fundamental advantages of this approach include its capability to provide a multi-disciplinary and multi-fidelity assessment of the engine behavior at an affordable computational cost, its suitability to be applied to CFD computations of airframe-engine configurations and the possibility to drive the coupling by specifying only one engine performance parameter.

The coupled approach has been validated against reference thermodynamic cycle calculations and subsequently demonstrated in the assessment of BLI impacts on the DGEN 380 turbofan operation for several thrust level requirements. Engine performance results highlight that although fan efficiency is penalized and surge margin decreased, reduced inlet momentum provides savings in engine power and thrust specific fuel consumption for a given net thrust level. Three-dimensional fan stage flow analysis reveals that fan-induced flow redistribution effects are responsible for core inlet distortion, which might have negative consequences in engine operability.

Future work will focus on applying this approach to investigate the potential gains of BLI in aircraft-engine configurations, thus accounting for the aerodynamic coupling effects between the engine and the airframe.

Acknowledgments

Airbus is gratefully acknowledged for the support provided during this study.

References

[1] Smith, L. H., "Wake Ingestion Propulsion Benefit," *Journal of Propulsion and Power*, Vol. 9, No. 1, 1993, pp. 74–82.

[2] Drela, M., "Power Balance in Aerodynamic Flows," *AIAA journal*, Vol. 47, No. 7, 2009, pp. 1761–1771.

[3] Hall, D. K., Huang, A. C., Uranga, A., Greitzer, E. M., Drela, M., and Sato, S., "Boundary Layer Ingestion Propulsion Benefit for Transport Aircraft," *Journal of Propulsion and Power*, Vol. 33, No. 5, 2017, pp. 1118–1129.

[4] Felder, J., Kim, H., and Brown, G., "Turboelectric Distributed Propulsion Engine Cycle Analysis for Hybrid-Wing-Body Aircraft," *47th AIAA aerospace sciences meeting including the new horizons forum and aerospace exposition*, 2009, p. 1132.

[5] Hardin, L., Tillman, G., Sharma, O., Berton, J., and Arend, D., "Aircraft System Study of Boundary Layer Ingesting Propulsion," *In 48th AIAA/ASME/SAE/ASEE Joint Propulsion Conference & Exhibit (p. 3993).*, 2012.

[6] Welstead, J., and Felder, J. L., "Conceptual Design of a Single-Aisle Turboelectric Commercial Transport with Fuselage Boundary Layer Ingestion," *54th AIAA Aerospace Sciences Meeting*, 2016, p. 1027.

[7] Gray, J. S., Mader, C. A., Kenway, G. K., and Martins, J., "Approach to Modeling Boundary Layer Ingestion using a Fully Coupled Propulsion-RANS Model," *In 58th AIAA/ASCE/AHS/ASC Structures, Structural Dynamics, and Materials Conference (p. 1753).*, 2017.

[8] Fidalgo, V. J., Hall, C., and Colin, Y., "A Study of Fan-Distortion Interaction within the NASA Rotor 67 Transonic Stage," *Journal of Turbomachinery*, Vol. 134, No. 5, 2012, p. 051011.

[9] Gunn, E. J., and Hall, C., "Aerodynamics of Boundary Layer Ingesting Fans," *ASME Turbo Expo 2014: Turbine Technical Conference and Exposition*, 2014.

[10] Carrier, G., Atinault, O., Grenon, R., and Verbecke, C., "Numerical and Experimental Aerodynamic Investigations of Boundary Layer Ingestion for Improving Propulsion Efficiency of Future Air Transport," *In 31st AIAA Applied Aerodynamics Conference (p. 2406)*, 2013.

[11] Blumenthal, B., Elmiligui, A. A., Geiselhart, K., Campbell, R. L., Maughmer, M. D., and Schmitz, S., "Computational Investigation of a Boundary Layer Ingestion Propulsion System for the Common Research Model," *46th AIAA Fluid Dynamics Conference*, 2016, p. 3812.

[12] Plas, A., Crichton, D., Sargeant, M., Hynes, T., Greitzer, E., Hall, C., and Madani, V., "Performance of a Boundary Layer Ingesting (BLI) Propulsion System," *45th AIAA aerospace sciences meeting and exhibit*, 2007, p. 450.

[13] Hall, D. K., "Analysis of Civil Aircraft Propulsors with Boundary Layer Ingestion," Ph.D. thesis, Massachusetts Institute of Technology, 2015.

[14] Thollet, W., "Body-Force Modeling of Fan-Airframe Interactions," Ph.D. thesis, ISAE-SUPAERO, 2017.

[15] López de Vega, L., Dufour, G., Blanc, F., and Thollet, W., "A Machine Learning Based Body Force Model for Analysis of Fan-Airframe Aerodynamic Interactions," *In Proceedings of GPPS Forum 18. Montreal, 7th-9th May*, 2018.

[16] Wiart, L., and Negulescu, C., "Exploration of the Airbus "Nautilius" Engine Integration Concept," *In ICAS 2018: 31st Congress of the International Council of the Aeronautical Sciences*, 2018.

[17] Follen, G., and AuBuchon, M., "Numerical Zooming Between a NPSS Engine System Simulation and a One-Dimensional High Compressor Analysis Code," *NASA-TM-209913*, 2000.

[18] Turner, M. G., Reed, J. A., Ryder, R., and Veres, J. P., "Multi-Fidelity Simulation of a Turbofan Engine with Results Zoomed into Mini-maps for a Zero-D Cycle Simulation," *In ASME Turbo Expo 2004: Power for Land, Sea, and Air (pp. 219-230)*, 2004.

[19] Claus, R. W., Lavelle, T., Townsend, S., and Turner, M., "Coupled High-Fidelity Engine System Simulation," *In 26th International Congress of the Aeronautical Sciences.*, 2008.

[20] Claus, R., Townsend, S., Lavelle, T., and Turner, M., "Coupled Component, Full Engine Simulation of a Gas Turbine Engine," *In 45th AIAA/ASME/SAE/ASEE Joint Propulsion Conference & Exhibit (p. 5017)*, 2008.

[21] Pachidis, V., Pilidis, P., Talhouarn, F., Kalfas, A., and Templalexis, I., "A Fully Integrated Approach to Component Zooming Using Computational Fluid Dynamics," *In ASME Turbo Expo 2005: Power for Land, Sea, and Air (pp. 191-199)*, 2005.

[22] Klein, C., Reitenbach, S., Schoenweitz, D., and Wolters, F., "A Fully Coupled Approach for the Integration of 3D-CFD Component Simulation in Overall Engine Performance Analysis," *In ASME Turbo Expo 2017: Turbomachinery Technical Conference and Exposition (pp. V001T01A014-V001T01A014)*, 2017.

[23] Klein, C., Wolters, F., Reitenbach, S., and Schönweitz, D., "Integration of 3D-CFD Component Simulation Into Overall Engine Performance Analysis for Engine Condition Monitoring Purposes," *In ASME Turbo Expo 2018: Turbomachinery Technical Conference and Exposition (pp. V001T01A013-V001T01A013)*, 2018.

[24] Pachidis, V., Pilidis, P., Marinai, L., and Templalexis, I., "Towards a Full Two Dimensional Gas Turbine Performance Simulator," *The Aeronautical Journal*, Vol. 111, No. 1121, 2007, pp. 433–442.

[25] Pilet, J., Lecordix, J. L., Garcia-Rosa, N., Barènes, R., and Lavergne, G., "Towards a Fully Coupled Component Zooming Approach in Engine Performance Simulation," *In ASME 2011 Turbo Expo: Turbine Technical Conference and Exposition (pp. 287-299)*, 2011.

[26] Alexiou, A., *Introduction to Gas Turbine Modelling with PROOSIS*, Empresarios Agrupados, 2015.

[27] Peters, A., "Ultra-Short Nacelles for Low Fan Pressure Ratio Propulsors," Ph.D. thesis, Massachusetts Institute of Technology, 2014.

[28] Meinel, M., and Einarsson, G. O., "The FlowSimulator Framework for Massively Parallel CFD Applications," *In PARA 2010 conference: state of the art in scientific and parallel computing.*, 2010.

[29] Benichou, E., Dufour, G., Bousquet, Y., Binder, N., Ortolan, A., and Carbonneau, X., "Body Force Modeling of the Aerodynamics of a Low-speed Fan Under Distorted Inflow," *In Proceedings of the 13th European Conference on Turbomachinery Fluid Dynamics & Thermodynamics, Lausanne, Switzerland; April 8-12*, 2019.

[30] Cambier, L., Heib, S., and Plot, S., "The Onera elsA CFD Software: Input from Research and Feedback from Industry," *Mechanics & Industry, 14(3), 159-174.*, 2013.

[31] Antares Development Team, "Antares Documentation Release 1.12.0," , 2012–2018. URL `https://cerfacs.fr/antares/`.

[32] Cumpsty, N., and Horlock, J., "Averaging Nonuniform Flow for a Purpose," *Journal of Turbomachinery*, Vol. 128, No. 1, 2006, pp. 120–129.